

## ExploreNEOs. II. THE ACCURACY OF THE WARM *SPITZER* NEAR-EARTH OBJECT SURVEY

A. W. HARRIS<sup>1</sup>, M. MOMMERT<sup>1</sup>, J. L. HORA<sup>2</sup>, M. MUELLER<sup>3</sup>, D. E. TRILLING<sup>4</sup>, B. BHATTACHARYA<sup>5</sup>,  
W. F. BOTTKE<sup>6</sup>, S. CHESLEY<sup>7</sup>, M. DELBO<sup>3</sup>, J. P. EMERY<sup>8</sup>, G. FAZIO<sup>2</sup>, A. MAINZER<sup>7</sup>,

B. PENPRASE<sup>9</sup>, H. A. SMITH<sup>2</sup>, T. B. SPAHR<sup>2</sup>, J. A. STANSBERRY<sup>10</sup>, AND C. A. THOMAS<sup>4</sup>

<sup>1</sup> DLR Institute of Planetary Research, Rutherfordstrasse 2, 12489 Berlin, Germany; alan.harris@dlr.de

<sup>2</sup> Harvard-Smithsonian Center for Astrophysics, 60 Garden Street, MS-65 Cambridge, MA 02138, USA

<sup>3</sup> Univ. de Nice Sophia Antipolis, CNRS, Obs. de la Côte d'Azur, BP 4229, 06304 Nice Cedex 4, France

<sup>4</sup> Department of Physics and Astronomy, Northern Arizona University, Flagstaff, AZ 86001, USA

<sup>5</sup> NASA Herschel Science Center, Caltech, M/S 100-22, 770 South Wilson Ave. Pasadena, CA 91125, USA

<sup>6</sup> Southwest Research Institute, 1050 Walnut St., Suite 300, Boulder, CO 80302, USA

<sup>7</sup> Jet Propulsion Laboratory, California Institute of Technology, Pasadena, CA 91109, USA

<sup>8</sup> Department of Earth and Planetary Sciences, University of Tennessee, 1412 Circle Dr., Knoxville, TN 37996, USA

<sup>9</sup> Department of Physics and Astronomy, Pomona College, 610 N. College Avenue, Claremont, CA 91711, USA

<sup>10</sup> Steward Observatory, University of Arizona, 933 North Cherry Avenue, Tucson, AZ 85721, USA

Received 2010 July 5; accepted 2010 November 29; published 2011 February 1

## ABSTRACT

We report on results of observations of near-Earth objects (NEOs) performed with the NASA *Spitzer Space Telescope* as part of our ongoing (2009–2011) Warm *Spitzer* NEO survey (“ExploreNEOs”), the primary aim of which is to provide sizes and albedos of some 700 NEOs. The emphasis of the work described here is an assessment of the overall accuracy of our survey results, which are based on a semi-empirical generalized model of asteroid thermal emission. The NASA *Spitzer Space Telescope* has been operated in the so-called Warm *Spitzer* mission phase since the cryogen was depleted in 2009 May, with the two shortest-wavelength channels, centered at 3.6  $\mu\text{m}$  and 4.5  $\mu\text{m}$ , of the Infrared Array Camera continuing to provide valuable data. The set of some 170 NEOs in our current Warm *Spitzer* results catalog contains 28 for which published taxonomic classifications are available, and 14 for which relatively reliable published diameters and albedos are available. A comparison of the Warm *Spitzer* results with previously published results (“ground truth”), complemented by a Monte Carlo error analysis, indicates that the rms Warm *Spitzer* diameter and albedo errors are  $\pm 20\%$  and  $\pm 50\%$ , respectively. Cases in which agreement with results from the literature is worse than expected are highlighted and discussed; these include the potential spacecraft target 138911 2001 AE<sub>2</sub>. We confirm that 1.4 appears to be an appropriate overall default value for the relative reflectance between the *V* band and the Warm *Spitzer* wavelengths, for use in correction of the Warm *Spitzer* fluxes for reflected solar radiation.

**Key words:** infrared: planetary systems – minor planets, asteroids: general – surveys

## 1. INTRODUCTION

The vast majority of near-Earth objects (NEOs) are thought to originate in collisions in the main asteroid belt (e.g., Morbidelli et al. 2002). A combination of orbital drift due to the momentum carried off by thermal photons and the gravitational influence of Jupiter causes the eccentricity of some collisional fragments to increase, moving their perihelia into the inner solar system; the term near-Earth object applies to those with perihelia within 1.3 AU of the Sun. NEOs are scientifically important due to, for example, the information they carry on the origin and mineralogy of asteroids in general, dynamical processes in the main belt, the relations between asteroids and comets, and asteroids and meteorites, and the influence impacts have had on the development of the planets, in particular Earth. Asteroids and comets may have supplied significant amounts of water and organic materials to the early Earth and thereby played a crucial role in the development of life (e.g., Drake & Righter 2002).

Collisions of NEOs with Earth have become less frequent since the end of the late heavy bombardment (about 3.8 Gyr ago) but the continued existence of a large and stable population of NEOs implies that many objects still find their way into the inner solar system replacing those that are lost by impacting the Sun or planets, or ejected as a result of close approaches to Jupiter. The residual impact hazard to modern civilization is small but scientifically well founded (Morrison et al. 2002),

providing another reason, albeit practical rather than scientific, for monitoring and characterizing the NEO population.

While robotic missions to NEOs have already taken place and more are planned, NEOs are also of increasing interest as feasible targets for manned space missions (Abell et al. 2009), providing a technical challenge of a magnitude between those of missions to the Moon and Mars. Vital prerequisites for any attempt to carry out a manned mission to an NEO, and maximize the usefulness of returned scientific data, are the identification of a suitable target asteroid and thorough characterization of its physical properties. A broad survey of the fundamental properties, such as size and albedo, of a large number of NEOs will greatly facilitate the task of target selection.

The current tally of NEO discoveries is more than 6700 (early 2010), of which, prior to our ExploreNEOs survey, the number with reliably determined diameters and albedos was around 90, i.e., a mere 1.3% (EARN database<sup>11</sup>). The rate of discoveries is still greatly outstripping the rate at which the population of NEOs can be physically characterized.

The NASA *Spitzer Space Telescope* (Werner et al. 2004) has been operated in the so-called Warm *Spitzer* mission phase since the cryogen was depleted in 2009 May. The two shortest-wavelength channels, centered at 3.6  $\mu\text{m}$  and 4.5  $\mu\text{m}$ , of the Infrared Array Camera (IRAC) continue to be useful for a

<sup>11</sup> <http://earn.dlr.de/>

number of observation programs. Our ExploreNEOs program of NEO observations with Warm *Spitzer* will deliver information on the sizes and albedos of some 700 NEOs, increasing the fraction of the known population for which these basic parameters have been measured from 1.3% to over 10%. In this work, we present an assessment of the accuracy of the ExploreNEOs Warm *Spitzer* results on the basis of the thermal-infrared data obtained and analyzed to date.

This paper is the second in the ExploreNEOs series, following the introductory paper (Trilling et al. 2010; hereafter ExploreNEOs I), which should be consulted for further background and general information on the ExploreNEOs program.

## 2. OBSERVATIONS AND DATA REDUCTION

The observational strategy and details of the data reduction techniques are presented in ExploreNEOs I, to which the reader is referred for more information; here we give a brief overview.

Each target was imaged in channels 1 and 2 (centered at  $3.550\text{ }\mu\text{m}$  and  $4.493\text{ }\mu\text{m}$ , with  $\lambda/\Delta\lambda = 4.7$  and 4.4, respectively) of the Infrared Array Camera, IRAC (Fazio et al. 2004), the only channels/wavelengths available in the *Spitzer* post-cryogenic phase. For more details, the reader is referred to the instrument-specific data handbook.<sup>12</sup>

The moving cluster astronomical observation template (AOT—a fixed observing pattern used by *Spitzer*) was used, tracking according to the standard NAIF ephemeris. The dithered observations alternated between the bandpasses during the observation to reduce the relative effects of any lightcurve variations within the observing period, and to maximize the relative motion of the asteroid to help reject background sources. The typical time between the end of one frame and the start of the following one (after offsetting, image transfer, and command overheads) was about 17 s.

The data were reduced using the IRACproc software (Schuster et al. 2006), which is based on the MOPEX routines provided by the *Spitzer Science Center* (Makovoz & Khan 2005). Mosaics of each astronomical observing request (AOR) were constructed using the “moving object mode,” which aligns the individual images in the rest frame of the moving target, based on its projected motion. Since the data are combined so that the NEO is at a fixed position in the final frame, the signal-to-noise ratio of the NEO is improved, whereas the background objects and transients are at different positions in the various frames. The outlier rejection in the mosaicking process then removes or minimizes the fixed background objects in the field and any transients due to cosmic rays or array artifacts. The images are rebinned to a pixel scale of  $0.8627\text{ arcsec pixel}^{-1}$  in the final mosaics.

We extracted the photometry using the *phot* task in IRAF. The noise in the image was estimated in the region near the NEO, and the extraction used an aperture radius of 6 mosaic pixels ( $5.176\text{ arcsec}$ ), with a sky annulus with inner radius of 6 pixels and outer radius of 12 pixels; these parameters are significantly smaller than the aperture size of 10 instrumental pixels ( $12.2\text{ arcsec}$ ) used in the IRAC calibration measurements (Reach et al. 2005). The smaller aperture was chosen to reduce the effects of background objects in the aperture in crowded fields where some of the NEOs were observed. In order to calibrate our NEO photometry, we extracted the photometry of IRAC calibration stars observed in the same campaigns as our NEO observations, at the same detector temperature and

bias settings. The same aperture sizes and sky annulus inner and outer radii were used for both the standard star and NEO. Measurements of the IRAC point-spread function to date have shown that its shape, and relative distribution between the core and outer regions, is not dependent on the brightness of the source, unless saturation is approached. The calibration stars and NEOs are measured well below saturation, so using the same aperture size for both is appropriate.

The observed asteroid flux contains reflected sunlight which must be subtracted before thermal models can be applied. The flux component from reflected sunlight was assumed to have the spectral shape of a  $5800\text{ K}$  black body over IRAC’s spectral range. The flux level was determined from the solar flux at  $3.6\text{ }\mu\text{m}$  ( $5.54 \times 10^{16}\text{ mJy}$ ; from the extraterrestrial solar spectrum of Gueymard 2004), the solar magnitude of  $V = -26.74$ , and the asteroid’s  $V$  magnitude as calculated from the observing geometry and the known  $H$  value. Reflected fluxes were multiplied by 1.4 to account for the increased reflectivity at  $3.6\text{ }\mu\text{m}$  and  $4.5\text{ }\mu\text{m}$  relative to the  $V$  band (e.g., Trilling et al. 2008; see Section 3.2).

The flux calibration as provided by the “basic calibrated data” (BCD) pipelines assumes a nominal source spectrum inversely proportional to wavelength. Since asteroid spectra do not conform to the assumed nominal source spectrum and the filter bandwidths are significant, color corrections have to be applied to the measured thermal fluxes to obtain monochromatic fluxes. Using the measured spectral response curves of IRAC, we determined color-correction factors for a typical NEO thermal-emission spectrum on the basis of a thermal model (NEATM, see Section 3), as described in Mueller et al. (2007) and ExploreNEOs I, that is, by convolving the thermal spectrum with the measured IRAC bandpasses. Since the shape of the thermal spectrum varies little from one target to another, the derived color-correction factors of 1.17 and 1.09 for  $3.6\text{ }\mu\text{m}$  and  $4.5\text{ }\mu\text{m}$ , respectively (where physical flux is equal to in-band fluxes divided by the color-correction factors), were applied throughout. Since the reflected solar flux components are very similar in shape to the nominal source spectrum assumed by the BCD pipelines, the corresponding correction factors are negligible.

With a few exceptions, the observational geometries, measured fluxes, and model results for the target set used here have been published in ExploreNEOs I. Further results will follow in subsequent publications.

## 3. THERMAL-MODEL FITTING

In order to derive sizes and albedos of asteroids from thermal-infrared observations a thermal model is required. The thermal emission observed at distance  $d$  from an atmosphereless spherical body is given by

$$F(\lambda) = \varepsilon R^2/d^2 \iint B[\lambda, T(\theta, \varphi)] \cos^2 \varphi \cos(\theta - \alpha) d\theta d\varphi, \quad (1)$$

where  $\varepsilon$  is the emissivity,  $R$  is the radius of the object,  $B$  is the Planck function,  $\varphi$  is the latitude,  $\theta$  is the longitude measured from the sub-solar point, and  $\alpha$  is the solar phase angle (e.g., Delbo’ & Harris 2002 and references therein). As is usual for asteroids, we adopt  $\varepsilon = 0.9$  throughout this work.

### 3.1. Applicable Models

The use of Equation (1) requires an assumed temperature distribution,  $T(\theta, \varphi)$ , over the surface. The standard thermal

<sup>12</sup> <http://ssc.spitzer.caltech.edu/irac>

model, STM (e.g., Lebofsky et al. 1986 and references therein), may be an appropriate model if the asteroid is rotating slowly and has a low thermal inertia (or its rotation axis points to the Sun) so that each surface element can be considered to be in instantaneous thermal equilibrium with insolation. Objects with significant loose, dusty regolith in poor thermal contact with the bulk mass of the object can be expected to display a low thermal inertia. A corresponding simple model for the extreme case of high thermal inertia and/or fast rotation is the so-called fast-rotating or isothermal-latitude model (Veeder et al. 1989; Lebofsky & Spencer 1989), hereafter ILM, in which the surface temperature distribution is a function of latitude only. An asteroid with a surface of bare rock would be expected to have a high thermal inertia.

The near-Earth asteroid thermal model, NEATM (Harris 1998), an extension of the STM, provides more accurate estimates of diameter and albedo in cases that are intermediate to those for which the STM and ILM are applicable. The STM and the NEATM both incorporate a so-called “beaming parameter”,  $\eta$ , which was originally introduced to allow the model temperature distribution to be modified from that of a smooth, zero-thermal-inertia sphere to take account of the observed enhancement of thermal emission at small solar phase angles due to surface roughness (“beaming”), i.e.,

$$T(\theta, \varphi) = T_{ss} \cos^{1/4}(\varphi) \cos^{1/4}(\theta) \quad (2)$$

in which the sub-solar temperature,  $T_{ss} = T_{(\theta=0, \varphi=0)}$ , is given by

$$T_{ss} = [(1 - A)S/(\eta \varepsilon \sigma)]^{1/4}, \quad (3)$$

where  $A$  is the bolometric Bond albedo,  $S$  is the solar flux at the asteroid, and  $\sigma$  is the Stefan-Boltzmann constant.  $A$  is related to the geometric albedo,  $p_V$ , and phase integral,  $q$ , via  $A \approx A_V = qp_V$  (Lebofsky & Spencer 1989). The phase integral is related to  $G$ , the slope parameter, via

$$q = 0.290 + 0.684G \quad (4)$$

(see Wisniewski et al. 1997 and references therein). Since we have no prior information on  $G$  for the vast majority of our targets, following ExploreNEOs I we adopt the default value  $G = 0.15$  throughout this work. In the refined STM of Lebofsky et al. (1986), designed for use with large main-belt asteroids and requiring measurements at only one thermal-infrared wavelength,  $\eta$  has the fixed value of 0.756. In contrast, the NEATM treats  $\eta$  as a variable, which modifies the color temperature, or flux distribution, of the model thermal continuum and enables it to be more accurately fitted to the measured continuum flux distribution. While the STM makes use of a fixed phase coefficient, the NEATM takes account of the phase angle by numerically integrating the observable thermal emission from the spherical surface illuminated by the Sun, assuming the surface emits with a Lambertian angular distribution. In the STM and the NEATM the temperature falls to zero at the terminator, and there is no thermal emission from the night side. Values of  $\eta$  resulting from NEATM best fits to NEO thermal-flux data generally lie in the range 0.65–3.0 (e.g., Delbo’ et al. 2003); values outside this range are incompatible with current understanding of asteroid surface roughness and thermal characteristics (e.g., Delbo’ 2004; Spencer et al. 1989).

For more detailed discussions of the NEATM and other thermal models outlined here, see Harris (1998, 2006), Delbo’ & Harris (2002), Harris & Lagerros (2002), Delbo’ et al. (2003),

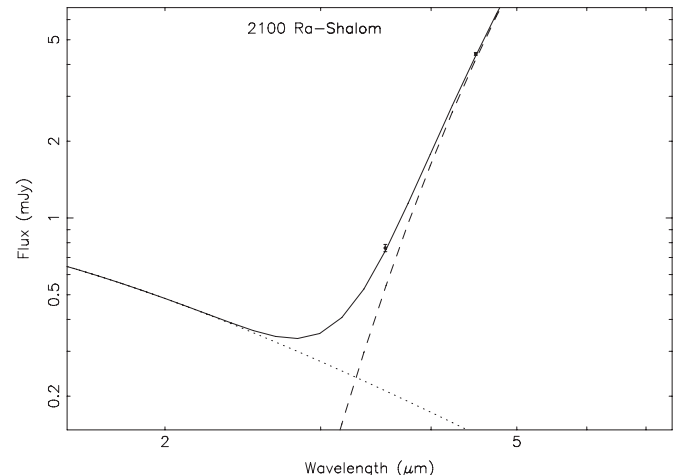


**Figure 1.** Thermal-emission (dashed curve) and reflected-solar (dotted curve) components fitted to the color-corrected Warm *Spitzer* fluxes for 2100 Ra-Shalom obtained in 2009 August. The continuous curve is the sum of the two components. Ra-Shalom is one of the targets for which the quality of the data enabled a two-point “floating- $\eta$ ” fit to be performed. The resulting diameter and albedo are in good agreement with earlier ground-based radar and infrared results (Shepard et al. 2008; Delbo et al. 2003). Note that the dotted curve derives from the solar spectrum assuming a temperature of 5800 K with no correction for the (unknown) wavelength-dependent reflectance of the asteroid’s surface; consequently, the data points have been adjusted downward to account for the assumed reflectance ratio of 1.4 (assumed to be the same for both channels, see the text) and avoid a discrepancy in the figure between the relative flux levels of the fitted components and the data points.

and references therein. Delbo’ & Harris (2002) give the mathematical expressions for calculating the wavelength-dependent observable thermal-infrared fluxes for all three models.

### 3.2. NEATM Usage: the Special Case of Warm Spitzer

In the case of the NEATM, a variable  $\eta$ , as opposed to the fixed  $\eta$  of the STM, allows a first-order correction for effects such as beaming, thermal inertia and rotation that influence the surface temperature distribution presented to the observer, and results in more accurate diameters and albedos. The value of  $\eta$  giving the best fit to the measured continuum flux distribution can be found via an iterative procedure, provided flux measurements at two or more well-spaced wavelengths are available (we refer to this as using the NEATM in “floating- $\eta$ ” mode). In the case of Warm *Spitzer*, only two channels, at 3.6  $\mu\text{m}$  and 4.5  $\mu\text{m}$ , are available and the flux in the 3.6  $\mu\text{m}$  channel is heavily contaminated with reflected solar radiation. Accurate subtraction of the reflected solar component would require knowledge of the visual to near-infrared relative reflectance of the surface material in each case, which varies according to spectral type and in general is not available for our targets. As described above, our compromise at present is to assume an IR/Vreflectance ratio of 1.4 (following Trilling et al. 2008 and ExploreNEOs I), based on the work of Rivkin et al. (1997) and Harris et al. (2009) for S-type asteroids. The ratio is assumed to be the same for both Warm *Spitzer* channels. Since the uncertainties in these assumptions are large, and floating- $\eta$  fits to the resulting Warm *Spitzer* thermal fluxes are often impossible or grossly inaccurate, we base our diameter and albedo estimates primarily on the 4.5  $\mu\text{m}$  measurement, which is largely uncontaminated by reflected solar radiation (e.g., see Figure 1), and use an empirical linear relation between  $\eta$  and the solar phase angle first demonstrated by Delbo’ et al. (2003) to provide an estimate of  $\eta$ . Wolters et al. (2008) have provided an updated relation including further observations,

deriving  $\eta = f(\alpha) = (0.013 \pm 0.004)\alpha + (0.91 \pm 0.17)$ , which is consistent with the results of Delbo' (2004) and is the relation used in this work.

Since the above procedure is largely untested, an urgent task is to investigate the overall reliability of the resulting diameters and albedos. The number of NEOs in the Warm *Spitzer* results database with reliable previously published diameters and albedos (14) is now large enough to allow a first assessment of the accuracy of our Warm *Spitzer* results.

#### 4. UNCERTAINTIES AND COMPARISON DATA

Uncertainties in thermal modeling usually exceed the formal errors resulting from the scatter of the flux measurements. Wright (2007) has tested the NEATM (in floating- $\eta$  mode) against a sophisticated thermophysical model and finds that it gives diameter estimates that are accurate to 10% rms for phase angles less than 60°, even for the non-spherical shapes typical of, for example, NEOs. Similar results were obtained by Delbo' (2004).

##### 4.1. Uncertainties in the Case of Warm *Spitzer*

The Warm *Spitzer* results are derived from an assumed linear relation between  $\eta$  and the solar phase angle ( $\eta = f(\alpha)$ ) and not by deriving  $\eta$  separately via model fitting to fluxes obtained at several wavelengths (floating- $\eta$  fit). The  $\eta = f(\alpha)$  approach is a reasonable compromise when only one flux measurement is available, but is likely to be significantly less accurate than the more robust floating- $\eta$  method when several good quality thermal-flux measurements are available. For any individual asteroid  $\eta$  may deviate significantly from the adopted  $\eta = f(\alpha)$  relation, depending on its (usually unknown) rotation vector, thermal inertia and surface roughness.

The uncertainties associated with absolute magnitudes ( $H$  values) contribute significantly to the error budget of the albedo results but normally have little effect on diameter uncertainties (Harris & Harris 1997; see Section 5.2 and Table 2). Furthermore, it is important to be aware of the rotational variability in observational data when applying thermal models. Some NEOs have rotational flux variability in excess of 1 mag. Therefore, in addition to systematic uncertainties in  $H$ , additional uncertainties are introduced from target lightcurves. In the case of Warm *Spitzer* observations, lightcurve-induced uncertainties are minimized for faint targets due to the relatively long integration times of up to 2000 s (Trilling et al. 2008; ExploreNEOs I), but for bright targets lightcurve-induced errors may contribute significantly to the overall error budget.

Overall uncertainties associated with diameters and albedos derived in our Warm *Spitzer* program have been estimated to be 25% and 50%, respectively (ExploreNEOs I). In the current work we test the validity of these uncertainty estimates by comparing the Warm *Spitzer* results with results from the literature, where available. We treat previously published results as “ground truth” and use the comparison to empirically estimate the overall uncertainties associated with the Warm *Spitzer* results.

##### 4.2. “Ground-truth” Data

A literature search was carried out to gather taxonomic classification, size, and albedo results for targets observed to date in our Warm *Spitzer* program (Table 1). A total of 28 of our targets have taxonomic classifications and 15 have previously

published sizes and albedos. Of the latter 15, we use 13 in our quantitative analysis, as discussed below. In all cases we believe the cited source gives the most reliable results, or the only results, available (cf. EARN database). In 10 out of the 13 cases results from the literature derive from multi-wavelength thermal-infrared observations and use of the NEATM fitted with floating  $\eta$ . In these cases, following Delbo' et al. (2003), Delbo' (2004) and Wolters et al. (2005), we assume that modeling errors dominate and assign overall uncertainties of 15% in diameter and 40% in albedo, whereby the latter includes an assumed uncertainty of 0.3 mag in  $H$  value (following ExploreNEOs I; e.g., see Parker et al. 2008).

In the cases of 1943 Anteros and 3103 Eger results are taken from Veeder et al. (1989), who calculate diameters and albedos on the basis of the STM and ILM from a number of 10  $\mu\text{m}$  flux measurements made at different phase angles. In the case of Eger, the diameters given by Veeder et al. are 1.4 km (STM) and 1.5 km (ILM). In the case of Anteros, the Veeder et al. (1989) diameter results are 1.8 km (STM) and 2.6 km (ILM). Since the STM and ILM address the two extremes of very low and very high thermal inertia and/or rotation rate (see Section 3.1), for the purposes of this study we take the mean of the STM and ILM results from Veeder et al. (1989), derive a modeling uncertainty from the difference between the STM and ILM results and add in quadrature the measurement uncertainty given by Veeder et al. The resulting uncertainties in diameter for Eger and Anteros are 13% and 20%, respectively; those for  $p_V$  are 40% and 50%, respectively.

The results in Table 1 for 2062 Aten are from Cruikshank & Jones (1977), who obtain very similar results to those of Morrison et al. (1976). In both cases, the results are based on an early version of the STM, which does not include the  $\eta$  parameter but uses a sub-solar temperature adjustment calibrated on the basis of observations of the Galilean satellites of Jupiter. The authors' quoted uncertainties are 20% in diameter and 33% in  $p_V$ .

For 2100 Ra-Shalom we take the results of Shepard et al. (2008), which are to our knowledge the most recent available. Shepard et al. show that their diameter result from multi-wavelength floating- $\eta$  NEATM fits agrees exactly with the size determined from radar data. The uncertainties quoted by Shepard et al. are within the conservative uncertainties adopted here for ground-truth results based on NEATM fits to multi-wavelength infrared data.

In the case of 1863 Antinous, Veeder et al. (1989) quote a diameter of 1.8 km and an albedo of 0.18 but from the information given it is not possible to check the reliability of these results; therefore, we have excluded Antinous from our quantitative analysis. Finally, we have also excluded 433 Eros from the quantitative analysis due to the unusual and unrepresentative geometric circumstances of the *Spitzer* observations (see ExploreNEOs I).

Note that any underestimation of the ground-truth uncertainties will lead to an overly pessimistic assessment of the accuracy of the Warm *Spitzer* results, since this is based on the rms difference between the two data sets.

#### 5. RESULTS AND DISCUSSION

Most of the Warm *Spitzer* albedos in Table 1 are consistent, given the uncertainties, with the approximate albedo ranges associated with the taxonomic classifications. Two cases of serious albedo/taxonomic class inconsistency are 138911 2001 AE<sub>2</sub> and 152637 1997 NC<sub>1</sub>. In both cases, the albedos are

**Table 1**  
Comparison of Results from Warm *Spitzer* and from the Literature for “Ground-truth” Targets

Asteroid	Warm <i>Spitzer</i>				Literature		Tax. Type and		Literature Sources
	D (km)	$p_V$	$\eta$	$\alpha$ ( $^{\circ}$ )	D (km)	$p_V$	Typical $p_V$ Range		
433 Eros ( $H = 11.16$ )	30.4	0.07	1.38	36.5	16.9	0.23	S 0.15–0.30	Thomas et al. (2002), Li et al. (2004)	
433 Eros ( $\eta = 1.07, H = 10.46$ )	23.0	0.22	1.07	36.5	24	0.23	S 0.15–0.30	Harris & Davies (1999), lightcurve max: $H = 10.46$	
1863 Antinous	3.16	0.11	1.99	83.3	...	...	Sq 0.15–0.45	Binzel et al. (2004)	
1943 Anteros	2.39	0.15	1.43	40.2	2.2	0.16	L 0.10–0.20	Veeder et al. (1989), Binzel et al. (2004)	
2062 Aten	1.30	0.20	1.91	76.6	0.94	0.18	S 0.15–0.30	Cruikshank & Jones (1977), Binzel et al. (2004)	
2100 Ra-Shalom	2.24	0.13	1.87	74.1	2.3	0.13	K 0.10–0.20	Shepard et al. (2008)	
3103 Eger	1.78	0.39	1.42	39.1	1.5	0.58	E, Xe 0.15–0.60	Veeder et al. (1989), Binzel et al. (2004)	
4183 Cuno	5.38	0.11	1.70	60.7	(4.5)	...	Sq 0.15–0.45	Binzel et al. (2004)	
4953 1990 MU	2.80	0.52	1.18	20.6	(3.6)	...	Q, R, S 0.15–0.45	Hicks et al. (1998), Whiteley (2001)	
4957 Brucemurray	3.01	0.18	1.36	34.7	(3.0)	...	S 0.15–0.30	Binzel et al. (2004)	
5143 Heracles	3.41	0.38	1.83	71.1	(5.0)	...	O, Sk 0.15–0.30	Binzel et al. (2004), Lazzarin et al. (2004)	
5604 1992 FE ( $H = 16.40$ )	0.84	0.69	1.86	73.3	0.55	0.48	V 0.20–0.50	Delbo et al. (2003) with $H = 17.72$ , Binzel et al. (2004)	
5604 1992 FE ( $H = 17.72$ )	0.65	0.35	1.86	73.3	0.55	0.48	V 0.20–0.50	Delbo et al. (2003) with $H = 17.72$ , Binzel et al. (2004)	
5626 1991 FE	3.87	0.15	1.34	33.1	(3.6)	...	S 0.15–0.30	Binzel et al. (2004)	
6455 1992 HE	4.01	0.33	1.23	24.5	3.55	0.26	S 0.15–0.30	Wolters et al. (2005), Binzel et al. (2004)	
7822 1991 CS	0.83	0.28	1.76	65.6	> 1.1	< 0.14	S 0.15–0.30	Benner et al. (1999), Binzel et al. (2004)	
7888 1993 UC	2.72	0.18	1.45	41.6	(3.1)	...	S, U 0.15–0.30	Whiteley (2001), Binzel et al. (2004)	
8566 1996 EN	1.25	0.28	1.57	50.6	(1.7)	...	U 0.15–0.30	Binzel et al. (2004)	
10302 1989 ML	0.24	0.49	1.64	56.0	0.28	0.37	E 0.30–0.60	Mueller et al. (2007)	
15745 1991 PM5	0.77	0.23	1.50	45.5	...	...	S 0.15–0.30	Binzel et al. (2004)	
16834 1997 WU22 ( $H = 15.7$ )	1.52	0.40	1.46	42.3	1.87	0.22	S 0.15–0.30	Delbo et al. (2003) with $H = 15.9$ , Binzel et al. (2004)	
16834 1997 WU22 ( $H = 15.9$ )	1.48	0.35	1.46	42.3	1.87	0.22	S 0.15–0.30	Delbo et al. (2003) with $H = 15.9$ , Binzel et al. (2004)	
17274 2000 LC16	5.04	0.014	1.66	57.9	(1.6)	...	Xk 0.03–0.20	Binzel et al. (2004)	
20826 2000 UV13	4.90	0.29	1.13	17.1	...	...	Sq 0.15–0.45	Binzel et al. (2004)	
36284 2000 DM8	3.08	0.19	1.66	57.4	...	...	Sq 0.15–0.45	Binzel et al. (2004)	
54686 2001 DU8	1.24	0.35	1.32	31.3	...	...	S 0.15–0.30	Binzel et al. (2004)	
65679 1989 UQ	0.72	0.06	1.67	58.6	(0.9)	...	B 0.04–0.15	Binzel et al. (2004)	
85989 1999 JD6	2.38	0.04	1.50	45.2	1.82	0.08	K 0.10–0.20	Camps et al. (2009), Binzel et al. (2004)	
108519 2001 LF	2.33	0.02	1.51	46.2	2.0	0.05	C 0.03–0.10	Delbo (2004) Dandy et al. (2003)	
138911 2001 AE2	0.35	0.34	1.45	41.8	...	...	T 0.04–0.10	Binzel et al. (2004)	
152637 1997 NC1	0.44	0.58	1.85	72.5	(1.4)	...	B 0.04–0.15	Whiteley (2001)	
184990 2006 KE89	1.25	0.28	1.63	55.7	1.78	0.15	...	Camps et al. (2009)	
1998 SV4	0.75	0.19	1.51	46.0	1.07	0.09	...	Camps et al. (2009)	
2004 XY60	0.47	0.19	1.71	61.8	0.40	0.28	...	Camps et al. (2009)	

**Notes.** The approximate ranges of typical  $p_V$  are based mainly on data from Bus (1999) and Tedesco et al. (1989). Diameters in brackets are derived from taxonomy-based albedo guesses (Binzel et al. 2002) and are very uncertain. 5604 and 16834 were observed by Delbo et al. (2003), who used newly derived  $H$  values (second entry in each case). The value  $H = 17.72$  for 5604 is 1.3 mag fainter than the  $H$  value given by *Horizons*; with the new  $H$  value, the Warm *Spitzer* results are more realistic. In the case of 433 Eros, the  $H$  value corresponding to lightcurve maximum, together with the appropriate  $\eta$  value, gives realistic results from the Warm *Spitzer* data (see ExploreNEOs I). The uncertainties in the diameter and albedo results from the literature are of the order of 15% and 40%, respectively (the uncertainties for Anteros and Aten differ slightly from these values—see Section 4.2). Insignificant differences between the  $D$  and  $p_V$  values given here and those given in ExploreNEOs I are due to improvements in the correction for reflected sunlight (see Section 2) in the analysis pipeline.

far higher than would be expected for a T- and a B-type asteroid, respectively (e.g., Bus 1999). Since proposals for NEO rendezvous missions tend to target primitive, carbonaceous (low-albedo) asteroids for scientific reasons, the case of 138911, which is relatively accessible ( $\Delta V = 4.22 \text{ km s}^{-1}$ ; Binzel et al. 2004) is of particular interest.

As mentioned above, a significant source of uncertainty in albedo estimates is the  $H$  value. In ExploreNEOs I, a typical  $H$ -value uncertainty of  $\sim 0.3$  mag was assumed (e.g., Parker et al. 2008), for the estimate of the total albedo uncertainty (we are pursuing a program of ground-based optical photometry to provide improved  $H$  values; in the meantime the  $H$  values in the Warm *Spitzer* results database are taken from the NASA JPL *Horizons* service). For consistency with the typical albedo ranges of a T- and a B-type asteroid (see Table 1), respectively, the  $H$  values of 138911 2001 AE<sub>2</sub> and 152637 1997 NC<sub>1</sub> would have to be increased by at least 1.5 mag and 2 mag. While it is evident from the examples of 433 Eros and 5604 1992 FE in Table 1 that our adopted  $H$  values can, in certain cases,

be erroneous by far more than 0.3 mag, we doubt that  $H$ -value errors are the explanation for the serious albedo/taxonomic class inconsistency in the cases of 138911 2001 AE<sub>2</sub> and 152637 1997 NC<sub>1</sub>. Another possible explanation is ambiguity in the taxonomic classification, due to inadequate spectral data or lack of distinguishing features in the available data. B- and T-type spectra are relatively featureless (e.g., Bus 1999), increasing the potential for misclassification in these cases. A discussion of taxonomic classification is beyond the scope of this paper, but a detailed comparison of taxonomic types and Warm *Spitzer* albedos will be the subject of a future ExploreNEOs paper (C. A. Thomas et al. 2011, in preparation).

Our results highlight 138911 2001 AE<sub>2</sub> and 152637 1997 NC<sub>1</sub> as interesting candidates for further analysis of existing spectroscopic data and/or for further infrared-photometric and spectroscopic observations in the future. The identification of taxonomic classifications that are inconsistent with Warm *Spitzer* albedo results will be an important contribution of the ExploreNEOs project.

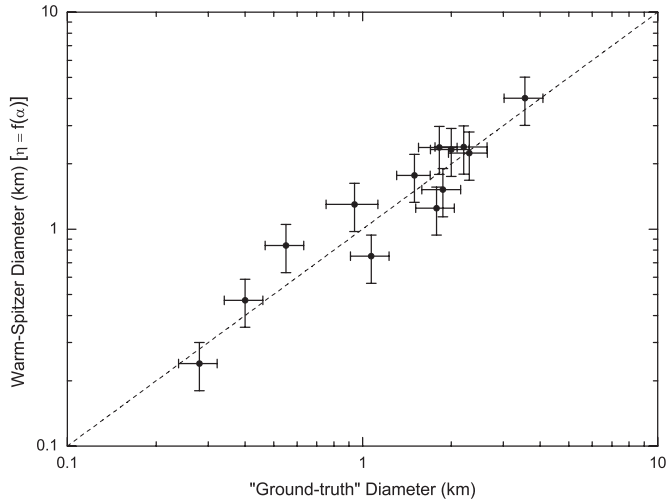


**Figure 2.** Warm *Spitzer* diameters compared to “ground-truth” results from the literature. The Warm *Spitzer* diameters were derived on the basis of the “fixed- $\eta$ ” method, which assumes a fixed linear relation between  $\eta$  and the solar phase angle ( $\eta = f(\alpha)$ , see the text). Error bars correspond to  $\pm 15\%$  and  $\pm 25\%$  for the literature and Warm *Spitzer* diameters, respectively.

### 5.1. Uncertainty Assessment from Comparison with “Ground-truth” Results

The Warm *Spitzer* diameters are compared with the corresponding values from the literature in Figure 2. Only unbracketed literature values in Table 1 are used. Error bars reflect originally estimated uncertainties of 25% in the case of the Warm *Spitzer* results, and 15% for the values from the literature. The mean fractional difference  $((D_{\text{ws}} - D_{\text{lit}})/D_{\text{lit}})$  is  $+8\%$  ( $\pm 7\%$ ), while the rms fractional difference is 26%. Assuming the ground-truth and Warm *Spitzer* flux measurements are independent, and the uncertainties in the diameter results largely random, we can estimate the rms uncertainty of the Warm *Spitzer* diameters by subtracting in quadrature the rms uncertainty in the ground-truth diameters (15%) from the rms fractional difference between the data sets (26%). The implied uncertainty in the Warm *Spitzer* diameters is  $\pm 21\%$ . While the current overlap of our Warm *Spitzer* results with results available in the literature is small, and the mean fractional diameter difference hardly significant, the value of  $+8\%$  may indicate a slight tendency to overestimation of sizes in the Warm *Spitzer* results. We explore the possibility that Warm *Spitzer* may overestimate sizes as a result of phase-angle-dependent modeling errors in Section 5.3.

Figure 3 shows the Warm *Spitzer* albedos compared to the corresponding values from the literature (data set as for Figure 2). Error bars reflect originally estimated uncertainties of 50% in the case of the Warm *Spitzer* results and 40% for the values from the literature. The Warm *Spitzer* albedos are taken directly from our current results database: no attempt has been made to ensure uniformity of  $H$  values between our database and results taken from the literature. In this way, we factor in some degree of realistic uncertainty in the  $H$  values. The mean fractional difference,  $(p_{V\text{ws}} - p_{V\text{lit}})/p_{V\text{lit}}$ , is  $+17\%$  ( $\pm 15\%$ ), while the rms fractional difference is 54%, which, assuming the uncertainty associated with the ground-truth albedos is  $\pm 40\%$ , suggests the rms uncertainty of the Warm *Spitzer* albedos is also about  $\pm 40\%$  (note that since the  $H$  values adopted by the literature sources and our values from *Horizons* are unlikely to be independent, the contribution of the uncertainty in  $H$  to the overall Warm *Spitzer* albedo uncertainty is probably

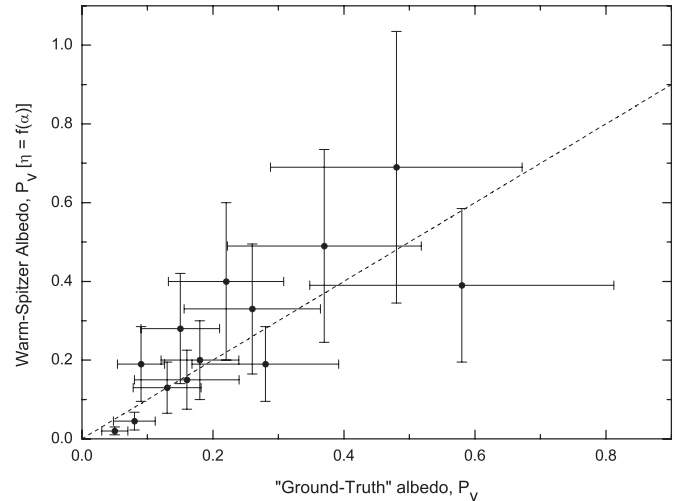


**Figure 3.** Warm *Spitzer* albedos compared to results from the literature (data set as in Figure 2). Error bars correspond to  $\pm 40\%$  and  $\pm 50\%$  for the literature and Warm *Spitzer* albedos, respectively.

underestimated here; we return to this point in the following section).

The possible slight tendency to overestimate sizes does not appear to be accompanied by a corresponding tendency to underestimate albedos; in fact, there may be an albedo bias in the opposite sense due to systematic differences in the  $H$  values adopted for the Warm *Spitzer* results (from the *Horizons* database) and those adopted by the authors of the ground-truth literature sources. The mean difference  $H_{\text{ws}} - H_{\text{GT}} = -0.185$  mag for the 13 objects in our quantitative analysis. Numerically lower  $H$  values give rise to higher albedos: a difference in  $H$  value of  $-0.185$  mag leads to an increase in albedo of about 18%, which is consistent with the result for the mean fractional albedo difference. The  $H_{\text{ws}} - H_{\text{GT}}$  differences in the cases of Anteros, Aten, and Eger, namely  $-0.25$ ,  $-0.80$ , and  $-0.08$  mag, are partly due to the authors quoting absolute magnitudes in a system predating the  $H, G$  system (corresponding absolute magnitudes in the  $H, G$  system are normally about 0.3 mag brighter; see Bowell et al. 1989). However, the mean  $H$ -value difference after excluding Anteros, Aten, and Eger from the data set is still  $-0.13$  mag and the corresponding albedo increase about 12% (note that the effect of this exclusion on the rms uncertainty of the Warm *Spitzer* albedos given above is negligible). This result emphasizes the significant contribution of  $H$ -value uncertainties to the overall error budget of the Warm *Spitzer* albedo results and the need for improved  $H$ -values for NEOs.

### 5.2. Uncertainty Assessment from a Monte Carlo Analysis

It is instructive to compare our overall uncertainty assessment from the previous section with an internal assessment of the uncertainties expected, given plausible errors in the choice of the parameters  $H, G, \eta$ , and  $\text{IR}/V$ . To this end we carried out a Monte Carlo analysis by generating, for each of the 13 objects used in our quantitative comparison with ground-truth results, 500 random sets of synthetic Warm *Spitzer* measured fluxes, and  $H, G, \eta$  and  $\text{IR}/V$  values, normally distributed about the values used in the original Warm *Spitzer* diameter and albedo derivations. We adopted the following  $1\sigma$  error ranges. Measured fluxes: from the ExploreNEOs database (see ExploreNEOs, Table 1);  $H$ :  $\pm 0.3$  mag;  $G$ :  $0.15 \pm 0.15$  (values of  $G$  outside the range

**Table 2**  
Relative Contributions to the Error Budget from a Monte Carlo Analysis

Parameter	Fractional Error in Diameter (%)	Fractional Error in Albedo (%)
Flux	3.3	7.5
$H$	3.3	27.6
$G$	1.6	3.5
$\eta$	18.4	41.6
IR/V	2.2	4.7
$\Sigma$ in quadrature	19.2	50.8

0.05–0.5 were considered atypical and excluded; cf. Wisniewski et al. (1997);  $\eta$ : from Wolters et al. (2008), see Section 3.2; IR/V:  $1.4 \pm 0.2$ . For each of the 500 sets of random data the corresponding diameter and albedo were calculated; the rms deviation from the mean in each case was taken as the resulting uncertainty.

The resulting fractional uncertainties are diameter: 19%, albedo: 51%, which are in good agreement with the results of the previous section (21% and 40%, respectively). As mentioned in the previous section, a smaller fractional albedo uncertainty would be expected from the comparison with the ground-truth results if, as is probable, the  $H$  values adopted by the authors of the ground-truth results and those adopted in the Warm *Spitzer* project are not independent.

Relative contributions to the error budget were explored by repeating the Monte Carlo exercise while keeping all but one error source fixed. The results are presented in Table 2. It is seen that in the case of diameter the dominant source of uncertainty by far is the  $\eta$  value. In the case of albedo, as expected (cf. Section 5.1), the  $H$  value also contributes significantly to the error budget. On the other hand, the contributions from all the other sources of error considered are small in comparison.

### 5.3. Uncertainty as a Function of Solar Phase Angle

In Section 4, it was mentioned that the NEATM has been tested against sophisticated thermophysical models and found to provide diameters accurate to within 10% for solar phase angles of up to  $\alpha = 60^\circ$ . At higher phase angles we would expect a tendency for the NEATM to overestimate diameters and, correspondingly, to underestimate albedos, due to the

assumption that the temperature falls to zero at the terminator, i.e., no thermal flux originates from the night side. Objects having significant thermal inertia and rotation axes oriented away from the solar direction would carry some thermal energy over to the night side. With increasing solar phase angle the proportion of the measured flux originating from the night side would increase, leading to larger diameters, and smaller albedos, being required for the NEATM fit. The magnitude of the resulting error depends on the thermal inertia, the rotation rate and sense, and the orientation of the rotation axis (for objects spinning pole-on to the Sun, the error is zero, regardless of thermal inertia or rotation rate/sense). While the magnitude of the error will vary widely from object to object, we would expect an overall tendency to overestimate diameters at phase angles beyond  $60^\circ$ .

We explore possible phase-angle-dependent errors with the help of Figures 4 and 5. The absolute fractional difference in diameter between the Warm *Spitzer* results and results from the literature is plotted as a function of solar phase angle,  $\alpha$ , in Figure 4. We note that both the ground-truth and the Warm *Spitzer* data sets would be expected to suffer from the phase-angle-dependent bias described above. However, since the phase angles at which the ground-truth and Warm *Spitzer* observations were made are in general not correlated, the comparison shown in Figure 4 is still valid. In particular, the ground-truth observations of the three objects in Figure 4 for which  $\alpha$  is larger than  $70^\circ$  were made at  $\alpha \leq 40^\circ$ , at which any diameter overestimation error should be relatively small. No significant trend to overestimation of diameters at  $\alpha > 60^\circ$  can be formally claimed in Figure 4, although the small number of data points precludes any robust conclusion. In particular, the fractional error in the case of 2100 Ra-Shalom, for which  $\alpha =$

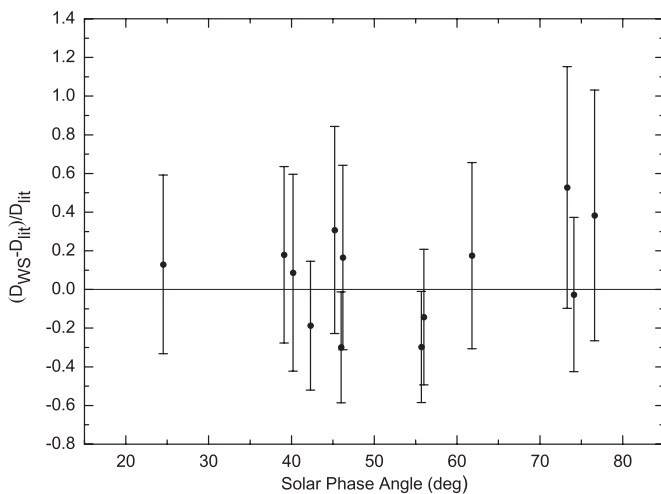


**Figure 4.** Fractional difference between Warm *Spitzer* diameters,  $D_{WS}$ , and diameters from the literature,  $D_{lit}$ , vs. solar phase angle,  $\alpha$ , of the Warm *Spitzer* observations (data set as for Figure 2). Error bars correspond to  $\pm 15\%$  and  $\pm 25\%$  for the literature and Warm *Spitzer* diameters, respectively.

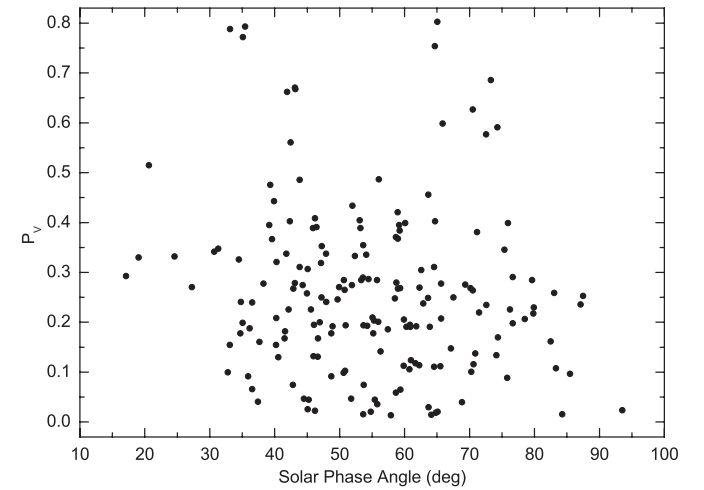


**Figure 5.** Albedo vs. solar phase angle,  $\alpha$ , for the current Warm *Spitzer* results catalog.

$74^\circ$ , is almost zero. The ground-truth for Ra-Shalom derives from the thermal-infrared and radar observations of Shepard et al. (2008) and should be among the most accurate ground-truth results in Table 1. Warm *Spitzer* albedo results are plotted against phase angle in Figure 5. No significant dependence of albedo on phase angle is apparent. These results suggest that the phase-angle-dependent bias described above is not a major contributor to the Warm *Spitzer* error budget.

While there is no significant evidence in the current data set for a phase-angle dependence of the tendency to overestimate sizes, a larger data set will be required to confirm the magnitude and nature of this bias. A further possible source of bias is the  $\eta = f(\alpha)$  relation of Wolters et al. (2008), which may require refinement. Investigating the magnitude of any systematic errors and the modification of analysis techniques to mitigate against them will remain an important task as the ExploreNEOs program progresses. In any case, the availability of reliable  $H$  values would reduce the uncertainty in the albedo results significantly.

As more Warm *Spitzer* data are gathered, we will continue to review the issues regarding uncertainties raised here in order to maximize accuracy and establish robust error estimates in the final Warm *Spitzer* database.

#### 5.4. Floating- $\eta$ Results and the Correction for Reflected Solar Radiation

While our main Warm *Spitzer* results database depends primarily on the  $4.5\ \mu\text{m}$  flux measurement, for which the correction for reflected solar radiation is small, the reflected contribution at  $3.6\ \mu\text{m}$  is very significant. Since there is very little information available on the relative reflectance between the  $V$  band and the Warm *Spitzer* wavelengths ( $\text{IR}/V$ ), our corrected  $3.6\ \mu\text{m}$  thermal fluxes are inevitably very uncertain. As discussed in Section 3.2, we have adopted a default value  $\text{IR}/V = 1.4$  based on previous work. Since  $\text{IR}/V$  varies with taxonomic class, the general applicability of this value to the Warm *Spitzer* targets cannot be taken for granted. For instance, since many asteroids have relatively flat, featureless  $V$ –IR spectra (e.g., B, C, X taxonomic types; Bus & Binzel 2002; Binzel et al. 2004) we might expect  $\text{IR}/V$  to be less than 1.4 in these cases. We examine the overall applicability of our assumption that  $\text{IR}/V = 1.4$  by using NEATM in floating- $\eta$  mode on the corrected thermal fluxes at  $3.6\ \mu\text{m}$  and  $4.5\ \mu\text{m}$  to derive  $\eta$  versus  $\alpha$  distributions, which we compare with the  $\eta = f(\alpha)$  relation of Wolters et al. (2008) based on results from the literature. In order to minimize the impact of possible large errors in the  $3.6\ \mu\text{m}$  thermal-flux values, we exclude  $4.5/3.6\ \mu\text{m}$  thermal-flux ratios that imply unrealistically high or low surface temperatures for the heliocentric distances, albedos and solar phase angles of the Warm *Spitzer* targets, and  $\eta$  values outside the range 0.65–3.0 (see Section 3.1). The resulting plots shown in Figure 6 demonstrate that with  $\text{IR}/V = 1.4$  the  $\eta$  distribution is reasonably consistent with that expected from results in the literature, given the uncertainties. In contrast, the assumption of flat  $V$ –IR reflectance, i.e.,  $\text{IR}/V = 1.0$  (Figure 6, lower frame), leads to a distribution of  $\eta$  biased to low values, compared to that expected from the  $\eta = f(\alpha)$  relation of Wolters et al. (2008). Furthermore, the plot for  $\text{IR}/V = 1.0$  has fewer points, because there are more cases of unrealistic  $4.5/3.6\ \mu\text{m}$  thermal-flux ratios and  $\eta$  values if  $\text{IR}/V = 1.0$  is adopted. These results may reflect the mix of taxonomic types in the Warm *Spitzer* sample to date, suggesting that we have relatively few dark, carbonaceous targets in our data set (since our Warm *Spitzer* target list is based on discoveries made with optical telescopes,

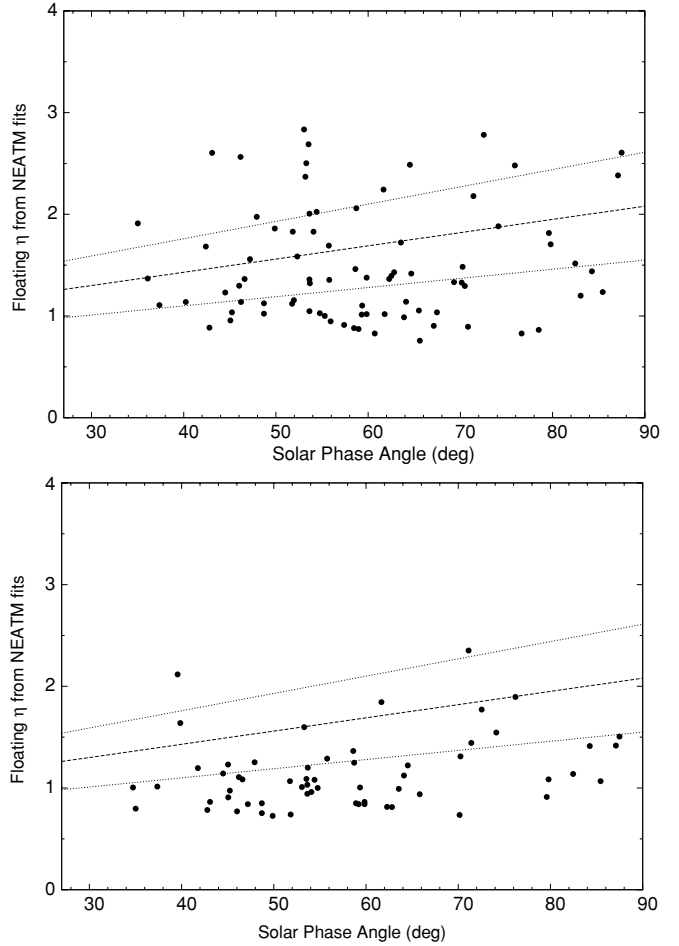


**Figure 6.** Upper frame: plot of the NEATM model parameter,  $\eta$  (from floating- $\eta$  fits to the Warm *Spitzer* corrected thermal-flux data at  $3.6\ \mu\text{m}$  and  $4.5\ \mu\text{m}$ ) against solar phase angle,  $\alpha$ , taking our adopted default reflectance ratio  $\text{IR}/V = 1.4$ . The dashed and dotted lines represent the Wolters et al. (2008) relation ( $\eta = (0.013 \pm 0.004) \alpha + (0.91 \pm 0.17)$ ) derived from fitting to results from the literature and used to estimate appropriate  $\eta$  values in the Warm *Spitzer* analysis (see Section 3.2). Lower frame: same as above, but for  $\text{IR}/V = 1.0$ . The plots demonstrate that the adopted correction for reflected solar radiation, which assumes  $\text{IR}/V = 1.4$ , leads to a realistic spread in  $\eta$  reasonably compatible with that expected from results in the literature; this is clearly not the case for  $\text{IR}/V = 1.0$ . The data have been filtered to exclude unrealistic  $\eta$  values and  $4.5/3.6\ \mu\text{m}$  thermal-flux ratios (see the text).

a bias against optically dark objects is not surprising). On the other hand, floating- $\eta$  results for low-albedo objects are less sensitive to the correction for reflected solar radiation (e.g., 2100 Ra-Shalom, which has  $p_V = 0.13$ , Figure 7), so it seems reasonable in any case to bias the adopted  $\text{IR}/V$  to that applicable to high-albedo, in particular S-type, objects.

For targets with relatively reliable ground-truth results we can check the validity of our adopted value of  $\text{IR}/V$  by comparing our resulting NEATM floating- $\eta$  diameters with the published values for a range of  $\text{IR}/V$ . Figure 7 shows the results of this exercise for 2100 Ra-Shalom. The absolute fractional difference between the NEATM floating- $\eta$  diameter and the ground-truth value has a minimum at  $\text{IR}/V = 1.45$ , which is close to our adopted value. A similar exercise in the case of 5604 1992 FE (with  $H = 17.72$ , see Table 1) leads to  $\text{IR}/V = 1.40$ . In the case of 433 Eros a value of 1.65 has been obtained from spectroscopic observations (ExploreNEOs I; J. P. Emery et al. 2011, in preparation). It should be noted in this context that the assumed value of  $G$  significantly influences the correction

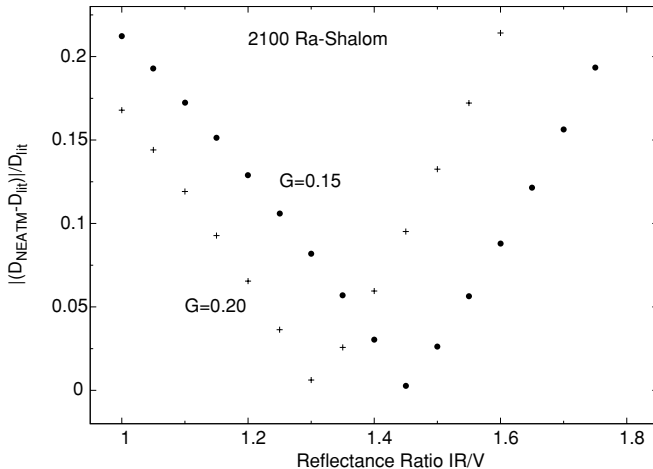


**Figure 7.** Absolute fractional difference between the NEATM floating- $\eta$  diameter and the ground-truth value ( $D = 2.3$  km) for 2100 Ra-Shalom as a function of the reflectance ratio,  $IR/V$ . The calculation of the reflected solar radiation flux components in this work assumes  $G = 0.15$  by default (filled circles). The reflectance ratio and  $G$  are interdependent in the sense that adoption of a different  $G$  value leads to a change in the value of  $IR/V$  at which the minimum occurs. For example, if  $G = 0.2$  (crosses) is adopted the minimum shifts from  $IR/V = 1.45$  to  $IR/V = 1.32$ . In other words, to maintain consistency between the NEATM floating- $\eta$  diameter and the ground-truth diameter a change in  $G$  has to be accompanied by a corresponding change in  $IR/V$ .

for reflected solar radiation, which is calculated for the relevant solar phase angle on the basis of the assumed  $H$  value (see Section 2). We adopt by default  $G = 0.15$  throughout this work (Section 3.1); if for any target the applicable  $G$  value differs significantly from 0.15, the appropriate value of  $IR/V$  has to be modified accordingly. For example, if  $G = 0.2$  is adopted in the case of Ra-Shalom, the minimum in Figure 7 shifts from  $IR/V = 1.45$  to  $IR/V = 1.32$ .

In summary, while the  $IR/V$  reflectance ratio would be expected to vary with taxonomic class, it seems the adopted value of 1.4 is a reasonable overall default value, at least for the set of targets observed to date. As the ExploreNEOs project progresses, the Warm *Spitzer* results will enable these conclusions to be refined and the relative reflectance,  $IR/V$ , to be investigated as a function of albedo and/or taxonomic class, thus providing insight into the reflectance properties of NEOs, and facilitating more robust corrections for reflected solar radiation and more accurate application of thermal models.

## 6. CONCLUSIONS

We have carried out a detailed comparison of the Warm *Spitzer* albedo/size results obtained to date with results available in the literature (“ground truth”). On the basis of a data set of 13 Warm *Spitzer* targets with apparently good-quality results available in the literature, we find the rms fractional difference between Warm *Spitzer* diameters and the literature values is 26%. The corresponding rms fractional albedo difference is 54%. Taking into account the uncertainties associated with the diameters and albedos from the literature, our results indicate that the rms error of the Warm *Spitzer* diameters is about  $\pm 20\%$ , and that of the Warm *Spitzer* albedos is at least  $\pm 40\%$ . Due to the limited overlap of the current Warm *Spitzer* data set with the current data set of objects having reliable ground truth, the results presented here should be considered preliminary pending more robust analyses based on larger data sets.

A Monte Carlo analysis performed on the same data set and based on realistic error ranges for the parameters  $H$ ,  $G$ ,  $\eta$ , and

the relative reflectance between the  $V$  band and the Warm *Spitzer* wavelengths,  $IR/V$ , gives rms errors of  $\pm 19\%$  and  $\pm 51\%$  for the Warm *Spitzer* diameters and albedos, respectively. The results of the Monte Carlo analysis demonstrate that the contributions to the overall error budget of  $G$  and  $IR/V$  are small in comparison to those of  $\eta$  and, in the case of albedo,  $H$ .

We find no evidence in the current Warm *Spitzer* data set for a significant phase-angle-dependent bias due to our procedure neglecting night-side thermal emission.

We have identified only two objects, in our data set of 28 with taxonomic classifications, for which the Warm *Spitzer* albedos lie well outside the ranges expected for their taxonomic classes, namely 138911 2001 AE<sub>2</sub> (a potential spacecraft target) and 152637 1997 NC<sub>1</sub>. In both cases, the albedos are higher by up to an order of magnitude than would be expected for a T- and a B-type asteroid, respectively. An explanation in terms of errors in  $H$  values seems unlikely. We flag these objects as interesting candidates for further analysis of existing spectroscopic data and/or for further infrared-photometric and spectroscopic observations.

We have confirmed the validity of the assumption that 1.4 is an appropriate overall default value for  $IR/V$ , for use in correction of the Warm *Spitzer* fluxes for contamination by reflected solar radiation. The assumption of a flat  $V$ –IR spectral form, i.e.,  $IR/V = 1.0$ , does not lead to a realistic distribution of  $\eta$  from floating- $\eta$  NEATM fits. Future investigations of the dependence of the  $IR/V$  reflectance ratio on albedo and/or taxonomic class may provide valuable insight into the near-infrared spectral properties of asteroids.

This work is based on observations made with the *Spitzer Space Telescope*, which is operated by the Jet Propulsion Laboratory, California Institute of Technology under a contract with NASA. Liberal use was made of the excellent JPL Horizons System for generating ephemerides. We acknowledge support by DFG through SPP 1385: The first ten million years of the solar system—a planetary materials approach. We thank the anonymous referee for comments that led to significant improvements in the paper.

## REFERENCES

- Abell, P. A., et al. 2009, *Meteorit. Planet. Sci.*, **44**, 1825
- Benner, L. A. M., et al. 1999, *Icarus*, **137**, 247
- Binzel, R. P., Lupishko, D. F., Di Martino, M., Whiteley, R. J., & Hahn, G. J. 2002, in *Asteroids III*, ed. W. F. Bottke et al. (Tucson, AZ: Univ. Arizona Press), **255**
- Binzel, R. P., Perozzi, E., Rivkin, A. S., Rossi, A., Harris, A. W., Bus, S. J., Valsecchi, G. B., & Slivan, S. M. 2004, *Meteorit. Planet. Sci.*, **39**, 351
- Binzel, R. P., Rivkin, A. S., Stuart, J. S., Harris, A. W., Bus, S. J., & Burbine, T. H. 2004, *Icarus*, **170**, 259
- Bowell, E., Hapke, B., Domingue, D., Lumme, K., Peltoniemi, J., & Harris, A. W. 1989, in *Asteroids II*, ed. R. P. Binzel, T. Gehrels, & M. S. Matthews (Tucson, AZ: Univ. Arizona Press), **524**
- Bus, S. J. 1999, PhD thesis, Massachusetts Institute of Technology
- Bus, S. J., & Binzel, R. P. 2002, *Icarus*, **158**, 146
- Camps, H., Kelley, M. S., Fernández, Y., Licandro, J., & Hargrove, K. 2009, *Earth Moon Planets*, **105**, 159
- Cruikshank, D. P., & Jones, T. J. 1977, *Icarus*, **31**, 427
- Dandy, C. L., Fitzsimmons, A., & Collander-Brown, S. J. 2003, *Icarus*, **163**, 363
- Delbo', M. 2004, Doctoral dissertation, Free Univ. Berlin, <http://www.diss.fu-berlin.de/2004/289/indexe.html>
- Delbo', M., & Harris, A. W. 2002, *Meteorit. Planet. Sci.*, **37**, 1929
- Delbo', M., Harris, A. W., Binzel, R. P., Pravec, P., & Davies, J. K. 2003, *Icarus*, **166**, 116
- Drake, M. J., & Righter, K. 2002, *Nature*, **416**, 39
- Fazio, G. G., et al. 2004, *ApJS*, **154**, 10
- Gueryard, C. A. 2004, *Sol. Energy*, **76**, 423

- Harris, A. W. 1998, *Icarus*, **131**, 291
- Harris, A. W. 2006, in Proc. IAU Symp. 229, ed. D. Lazzaro et al. (Cambridge: Cambridge Univ. Press), 449
- Harris, A. W., & Davies, J. K. 1999, *Icarus*, **142**, 464
- Harris, A. W., & Harris, A. W. 1997, *Icarus*, **126**, 450
- Harris, A. W., & Lagerros, J. S. V. 2002, in Asteroids III, ed. W. F. Bottke, A. Cellino, P. Paolicchi, & R. P. Binzel (Tucson, AZ: Univ. Arizona Press), 205
- Harris, A. W., Mueller, M., Lisse, C. M., & Cheng, A. F. 2009, *Icarus*, **199**, 86
- Hicks, M. D., Fink, U., & Grundy, W. M. 1998, *Icarus*, **133**, 69
- Lazzarin, M., Marchi, S., Barucci, M. A., Di Martino, M., & Barbieri, C. 2004, *Icarus*, **169**, 373
- Lebofsky, L. A., & Spencer, J. R. 1989, in Asteroids II, ed. R. P. Binzel, T. Gehrels, & M. S. Matthews (Tucson, AZ: Univ. Arizona Press), 128
- Lebofsky, L. A., et al. 1986, *Icarus*, **68**, 239
- Li, J., A'Hearn, M. F., & McFadden, L. A. 2004, *Icarus*, **172**, 415
- Makovoz, D., & Khan, I. 2005, in ASP Conf. Ser. 347, Astronomical Data Analysis Software and Systems XIV, ed. P. L. Shopbell et al. (San Francisco, CA: ASP), 81
- Morbidelli, A., Bottke, W. F., Froeschlé, Ch., & Michel, P. 2002, in Asteroids III, ed. W. F. Bottke, A. Cellino, P. Paolicchi, & R. P. Binzel (Tucson, AZ: Univ. Arizona Press), 409
- Morrison, D., Gradie, J. C., & Rieke, G. H. 1976, *Nature*, **260**, 691
- Morrison, D., Harris, A. W., Sommer, G., Chapman, C. R., & Carusi, A. 2002, in Asteroids III, ed. W. F. Bottke, A. Cellino, P. Paolicchi, & R. P. Binzel (Tucson, AZ: Univ. Arizona Press), 739
- Mueller, M., Harris, A. W., & Fitzsimmons, A. 2007, *Icarus*, **187**, 611
- Parker, A., Ivezić, Ž., Jurić, M., Lupton, R., Sekora, M. D., & Kowalski, A. 2008, *Icarus*, **198**, 138
- Reach, W. T., et al. 2005, *PASP*, **117**, 978
- Rivkin, A. S., Howell, E. S., Clark, B. E., Lebofsky, L. A., & Britt, D. T. 1997, *Lunar Planet. Sci.*, **28**, 1803, Abstract
- Schuster, M. T., Marengo, M., & Patten, B. M. 2006, *Proc. SPIE*, **6270**, 65
- Shepard, M. K., et al. 2008, *Icarus*, **193**, 20
- Spencer, J. R., Lebofsky, L. A., & Sykes, M. V. 1989, *Icarus*, **78**, 337
- Tedesco, E. F., Matson, D. L., & Veeder, G. J. 1989, in Asteroids II, ed. R. P. Binzel, T. Gehrels, & M. S. Matthews (Tucson, AZ: Univ. Arizona Press), 290
- Thomas, P. C., et al. 2002, *Icarus*, **155**, 18
- Trilling, D. E., et al. 2008, *ApJ*, **683**, L199
- Trilling, D. E., et al. 2010, *AJ*, **140**, 770 (ExploreNEOs I)
- Veeder, G. J., Hanner, M. S., Matson, D. L., Tedesco, E. F., Lebofsky, L. A., & Tokunaga, A. T. 1989, *AJ*, **97**, 1211
- Werner, M. W., et al. 2004, *ApJS*, **154**, 1
- Whiteley, R. J. 2001, PhD thesis, Univ. of Hawaii
- Wisniewski, W. Z., Michałowski, T. M., Harris, A. W., & McMillan, R. S. 1997, *Icarus*, **126**, 395
- Wolters, S. D., Green, S. F., McBride, N., & Davies, J. K. 2005, *Icarus*, **175**, 92
- Wolters, S. D., Green, S. F., McBride, N., & Davies, J. K. 2008, *Icarus*, **193**, 535
- Wright, E. L. 2007, *BAAS*, **39**, 483